A Finite Element Method for the Transient Electric Field by Using Indirect Laplace Transform with High Accuracy

Teng Wen, Xiang Cui, *Senior Member, IEEE*, Xuebao Li, *Member, IEEE*, Sijia Liu, and Zhibin Zhao, *Member, IEEE*.

***Abstract*—This paper focuses on the finite element method in the complex frequency domain (CFD-FEM) for the transient electric field. Firstly, the initial value- boundary value problem of the transient electric field under the electroquasistatic field in the complex frequency domain is given. Besides, the finite element equation and the constrained electric field equation on the boundary are derived. Secondly, the indirect algorithm of the numerical inverse Laplace transform is introduced. Based on it, the calculation procedures of the CFD-FEM are illustrated in detail. Thirdly, the step response, zero-state response under the positive periodic square waveform (PPSW) voltage, and the zero-input response by the CFD-FEM with direct algorithm and indirect algorithm are compared. Lastly, the reason for the numerical oscillations of the zero-state response under the PPSW voltage is analyzed, and the method to reduce oscillations is proposed. The results show that the numerical accuracy of the indirect algorithm of the CFD-FEM is more than an order of magnitude higher than that of the direct algorithm when calculating the step response of the transient electric field. The proposed method can significantly reduce the numerical oscillations of the zero-state response under the PPSW voltage. The proposed method is helpful for the calculation of the transient electric field, especially in the case of frequency-dependent parameters.**

***Index Terms*—electroquasistatic field, transient electric field, finite element method, complex frequency domain, numerical Laplace transform.**

I. Introduction

THE electrical insulation problem is often a critical challenge in the manufacturing process of power apparatus [1, 2]. The key to solving the insulation problem is to accurately calculate the electric field distribution of the insulation structure under actual working conditions. With the widespread application of power electronic devices in the power grid, the working voltage of high-voltage power electronic devices or equipment is no longer the traditional AC or DC voltage, but a positive periodic square waveform (PPSW) voltage [3, 4]. Besides, the insulation structure of the device or equipment is often a combined insulation structure composed of multiple materials [5]. Under the electroquasistatic (EQS) field, charge relaxation phenomena occur in the composite insulating structure, which leads to the transition process of the transient electric field, and finally reaches a steady state after a duration of time [6]. Therefore, it is essential to calculate the transient electric field distribution of the insulating structure under the EQS field.

The finite element method (FEM) is a useful numerical method for solving partial differential equations for the electric field, which is suitable for both regular and irregular structures [7]. For the calculation of the transient electric field, it is essential to deal with the partial derivative of time in the governing equation. In general, there are two kinds of methods to handle the partial derivatives of time. The first one is the time-domain method based on the time difference. Combined with FEM, many methods are produced, including time-domain FEM (FD-FEM) [8, 9], time-periodic FEM [10], and so on. The other one is the transformation method based on the integral transformation combined with FEM, including frequency-domain FEM (FD-FEM) [11, 12], and complex frequency domain FEM (CFD-FEM) [13, 14].

The transient response of the electric field can be easily obtained by TD-FEM through time iteration. But for composite insulation structures with a large time constant up to hundreds of seconds or even thousands of seconds. It will take a very long time to get the steady-state solution of the transient electric field, which needs tremendous calculation costs [6]. While the FD-FEM is based on the fast Fourier transform, by which the steady-state solution of the transient electric field can be obtained quickly. However, FD-FEM cannot obtain the transition process of the transient electric field, nor the zero-input response of the transient electric field originated by the initial state [15]. The CFD-FEM based on Laplace transform can make up for the drawbacks of the FD-FEM.

The CFD-FEM is based on the numerical Laplace inverse transform. The algorithms for the numerical inverse Laplace transform are mainly divided into two categories. The first one is the direct algorithm through the direct discretization of the

Manuscript received November **, 2020; revised April 2, 2018; accepted June 28, 2018. Date of publication December 30, 2018; date of current version November 15, 2018.

This work was supported by the National Natural Science Foundation of China (No. 52077073).

T. Wen, X. Cui, S. J. Liu, X. B. Li (corresponding author, e-mail: lxb08357x@ncepu.edu.cn), and Z. B. Zhao are with State Key Laboratory of Alternate Electrical Power System with Renewable Energy Sources, North China Electric Power University, Beijing 102206, China.

DOI: 10.17775/CSEEJPES.2021.07590

Bromwich contour integral [16-18]. The other one is the indirect algorithm through functional expansion using analytically invertible basis functions [19], including the Gaver-Stehfest method [20], Week method [21], Talbot method [22], Valsa method [23], and so on. The computational complexity of the direct algorithm is lower than the indirect algorithm. However, the numerical accuracy is greatly dependent on the attenuation coefficient. Besides, the numerical oscillations will be produced when calculating the zero-input response. Thus, it is essential to research the indirect algorithm. Among the indirect algorithms, the Valsa method is approximate the kernel of the inverse Laplace transform by the reciprocal hyperbolic functions, which is easy to control the absolute errors [24]. Thus, the Valsa method is widely used in groundwater flow [25] and solute transport [26].

This paper is devoted to the CFD-FEM through the indirect algorithm of the numerical inverse Laplace transform. Firstly, the finite element equation and the constrained electric field equation in the complex frequency domain are given. Secondly, the calculation procedures for the transient electric field by the CFD-FEM are proposed. Thirdly, the step response, zero-state response under the PPSW voltage, and the zero-input response by the CFD-FEM with direct algorithm and indirect algorithm are compared. Lastly, the reason for the numerical oscillations of the zero-state response under the PPSW voltage is analyzed, and the method to reduce oscillations is proposed. This paper provides a new method for the transient electric field.

II. Finite Element Equation Of Transient Electric Field In Complex Frequency Domain

The EQS approximation is effective when the characteristic length of the electromagnetic system is much smaller than the distance that the electromagnetic wave travels during the characteristic time of the electromagnetic system. The transient electric field of the high voltage devices and apparatus often satisfies the EQS condition, thus, the magnetic induction of Maxwell's equation can be neglected. As a result, the electric field is free of rotation approximately, and the scalar electric potential function φ can be introduced as $\boldsymbol{E}=-\nabla\varphi$, where $\boldsymbol{E}$ is electric field intensity.

A. Description of Initial Value – Boundary Value Problem

Under the EQS field, the governing equation of transient electric filed in time domain represented by scalar potential is expressed as [27]

$$-\nabla\bullet\left\{\gamma\nabla\varphi+\frac{\partial}{\partial t}(\varepsilon\nabla\varphi)\right\}=0 \tag{1}$$

where φ is scalar electric potential, ε and γ are permittivity and conductivity of the medium, respectively, and t is time.

Supposing the mediums are isotropic, linear, and uniform, by taking the Laplace transform of (1), the governing equation in the complex frequency domain can be obtained, which is

$$-\nabla\bullet\left\{\gamma\nabla\varphi_l(s)+\varepsilon\left[\nabla s\varphi_l(s)-\nabla\varphi_t(0_-)\right]\right\}=0 \tag{2}$$

where $\varphi_l(s)$ is the image function of φ in Laplace domain, $\varphi_t(0_-)$ is the initial condition of φ in the time domain, s is complex frequency, $s=c+\mathrm{j}\omega$, ω is the angular frequency, and c is a positive and real number, also named as decay coefficient.

The general domain and boundary for calculation are depicted in Fig. 1. Let field domain $\Omega\subset\mathbb{R}^2$ is a convex polygonal domain, the interface Γ_{12} separates Ω into two subdomains with different medium Ω_1 and Ω_2, thus $\Omega=\Omega_1\cup\Omega_2\cup\Gamma_{12}$. Let $\partial\Omega$ is the boundary of domain Ω, Γ_1 is the Dirichlet boundary, Γ_2 is the Neumann boundary, such that $\partial\Omega=\Gamma_1\cup\Gamma_2$.

For the general model in Fig. 1, the initial value and boundary value problem for scalar electric potential in the complex frequency domain can be expressed as

$$\begin{cases}\nabla\bullet\left\{\gamma\nabla\varphi_l(s)+\varepsilon\left[\nabla s\varphi_l(s)-\nabla\varphi_t(0_-)\right]\right\}=0\\ \varphi_l\big|_{\Gamma_1}=u_l(s)\\ \left.\dfrac{\partial\varphi_l}{\partial n}\right|_{\Gamma_2}=\psi_l(s)\\ \varphi_t(0_-)=\varphi(0)\end{cases} \tag{3}$$

where, $u_l(s)$ is the Laplace transform of the electric potential on the Dirichlet boundary, $\psi_l(s)$ is the Laplace transform of the derivative of the electric potential in the normal direction on the Neumann boundary, and $\varphi(0)$ is the initial value of the electric potential.

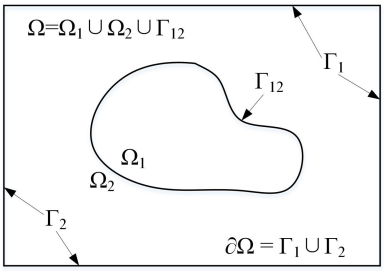

Fig. 1 A sketch of the domain and boundary[27]

B. FEM in Complex Frequency Domain

Discretizing the field domain into m finite elements with n nodes in Ω. Among m elements, m_1 elements are collinear with the Dirichlet boundary Γ_1, and m_2 elements are collinear with the Neumann boundary Γ_2. Assuming there are (n-n_1) nodes on the Dirichlet boundary Γ_1.

By using Galerkin's method, the weak form of (3) can be obtained. Then, by using Green's formula, the integral of the weak form can be decomposed into two parts, the integral for the field domain and the boundary, respectively. Considering physical meaning, $-\partial\varphi/\partial n$ stands for normal component of the electric field intensity E_n. Thus, the closed curve integral along the boundary in the right hand of the weak form can be divided into two parts. One is the curve integral along the Neumann boundary where $\partial\varphi/\partial n$ is given, and the other one is the curve integral along the Dirichlet boundary where $\partial\varphi/\partial n$ can be represented as $-E_n$. Thus, the finite element equation corresponding to (3) can be expressed as

$$\sum_{j=1}^{n}\left[\sum_{e=1}^{m}\int_{\Omega_e}(\gamma+\varepsilon s)\nabla N_i^e\bullet\nabla N_j^e\,\mathrm{d}\Omega\right]\varphi_{ij}(s)-\sum_{j=1}^{n}\left(\sum_{e=1}^{m}\int_{\Omega_e}\varepsilon\nabla N_i^e\bullet\nabla N_j^e\,\mathrm{d}\Omega\right)\varphi_{tj}(0_-)=\sum_{e=1}^{m_2}\int_{\Gamma_{2e}}(\gamma+\varepsilon s)N_i^e\psi(s)\,\mathrm{d}\Gamma-\sum_{e=1}^{m_1}\int_{\Gamma_{1e}}(\gamma+\varepsilon s)N_i^eE_{nl}(s)\,\mathrm{d}\Gamma-\sum_{e=1}^{m_2}\int_{\Gamma_{2e}}\varepsilon N_i^e\psi_t(0_-)\,\mathrm{d}\Gamma+\sum_{e=1}^{m_1}\int_{\Gamma_{1e}}\varepsilon N_i^eE_{nt}(0_-)\,\mathrm{d}\Gamma \tag{4}$$

where, n is the total number of nodes, m is the total number of elements, N^e_i is the base function for node i in element e.

The finite element equation (4) can be expressed as the matrix form

$$\mathbf{S}_k\mathbf{\Phi}_{lk}=\mathbf{T}\mathbf{\Phi}_t(0_-)+\mathbf{F}_k \tag{5}$$

where, $\mathbf{S}_k$ and $\mathbf{T}$ are stiffness matrixes, $\mathbf{F}_k$ is a vector of the boundary integrals in the right hand of (5), and $\mathbf{\Phi}$ is the column vector of the nodal potential. The expression of $\mathbf{S}_k$, $\mathbf{T}$, and $\mathbf{F}_k$ are expressed in the appendix

C. Constrained Electric Field Equation on the Boundary in Complex Frequency Domain

When numbering the nodes, nodes that are in Ω but not on the Γ_1 are numbered firstly. Then, nodes on the Γ_1 with given nodal potentials are numbered in sequence. As a result, (5) can be represented as partitioned matrixes

$$\mathbf{\Phi}_{lk}=\mathbf{S}_{k11}^{-1}\left[\mathbf{T}_{11}\mathbf{\Phi}(0_-)+\mathbf{T}_{21}^{\mathrm{T}}\mathbf{U}(0_-)+\mathbf{F}_{k2}-\mathbf{S}_{k21}^{\mathrm{T}}\mathbf{U}_{lk}\right] \tag{6}$$

$$\mathbf{F}_{k1}=\mathbf{S}_{k21}\mathbf{\Phi}_{lk}+\mathbf{S}_{k22}\mathbf{U}_{lk}-\mathbf{T}_{21}\mathbf{\Phi}(0_-)-\mathbf{T}_{22}\mathbf{U}(0_-) \tag{7}$$

where, $\mathbf{\Phi}$ is a column vector of the nodal potential which is needed to be solved, and $\mathbf{U}$ is a column vector of the nodal potential with known potential values on the Dirichlet boundary.

Equation (6) is the finite element equation for electric potential in the complex frequency domain, and (7) is the constrained electric field equation on the boundary in the complex frequency domain (CEFEB-CFD), which reflect the constraint relationship between the normal component of the transient electric field intensity and the transient potential.

Element values of column vector $\mathbf{F}_{k1}$ are expressed as

$$-f_{ki}=\sum_{e=1}^{m_1}\int_{\Gamma_{1e}}\left[\gamma+(c+\mathrm{j}2\pi k\Delta f)\varepsilon\right]N_i^eE_{nlk}\,\mathrm{d}\Gamma-\sum_{e=1}^{m_1}\int_{\Gamma_{1e}}\varepsilon N_i^eE_{ni}(0_-)\,\mathrm{d}\Gamma \tag{8}$$

Equation (8) can be expressed in the form of a matrix equation as

$$\mathbf{H}_k\mathbf{E}_{nlk}-\mathbf{G}\mathbf{E}_n(0_-)=-\mathbf{F}_{k1} \tag{9}$$

where, $\mathbf{E}_{nlk}$ is the column vector of the normal component of the electric field intensity on the Dirichlet boundary, $\mathbf{E}_n(0_-)$ is the Column vector consisting of the initial value of the normal component of the electric field intensity on the Dirichlet boundary, $\mathbf{H}_k$ and $\mathbf{G}$ are stiffness matrixes on the Dirichlet boundary corresponding to $\mathbf{E}_{nlk}$ and $\mathbf{E}_n(0_-)$, respectively. The expression of $\mathbf{H}_k$ and $\mathbf{G}$ are listed in the appendix.

By taking (9) into (7), CEFEB-CFD can be expressed as

$$\mathbf{E}_{nlk}=-\mathbf{H}_k^{-1}\left[\mathbf{S}_{k21}\mathbf{\Phi}_{lk}+\mathbf{S}_{k22}\mathbf{U}_{lk}-\mathbf{T}_{21}\mathbf{\Phi}(0_-)-\mathbf{T}_{22}\mathbf{U}(0_-)-\mathbf{G}\right] \tag{10}$$

Equation (10) is also named the CEFEB-CFD. After calculating the nodal potential in the complex frequency domain by (6), the normal component of the electric field intensity on the Dirichlet boundary in the complex frequency domain can be calculated by (10).

III. Indirect Algorithm of Numerical Laplace Transform

In the process of calculating the transient electric field by the CFD-FEM, one of the most important procedures is achieving the numerical inverse Laplace transform after obtaining the electric potential and the electric field in each complex frequency point by (6) and (10), respectively, to obtain the transient electric potential and the transient electric field in the time domain. As a result, the calculation algorithm of the numerical inverse Laplace transform should be introduced in this section in detail.

The inverse Laplace transform is defined by the Bromwich contour integral

$$f(t)=\frac{1}{\mathrm{j}2\pi}\int_{c-\mathrm{j}\infty}^{c+\mathrm{j}\infty}F(s)\mathrm{e}^{st}\mathrm{d}s \tag{11}$$

where $f(t)$ is the time function, and F(s) is the image function of $f(t)$ in the Laplace domain. In general, the image function $F(s)$ is supposed to fulfill the following assumptions:

(a) Re[s]>0, (b) $F(s)$=0 when $|s|\to\infty$, (c) $F^*(s)$= $F(s^*)$, where the asterisk stands for complex conjugate value.

To approximate the kernel of exp(st) in the expression of inverse Laplace transform (11), the damping factor a is introduced, where a is a positive and real parameter. When $a > ct$, then $|\mathrm{e}^{-2a}\mathrm{e}^{2st}\ll 1|$. Thus, the kernel of the inverse Laplace transform exp(st) can be approximated by

$$\mathrm{e}^{st}\doteq\frac{\mathrm{e}^{a}}{2\cosh(a-st)}=\frac{\mathrm{e}^{st}}{1+\mathrm{e}^{-2a}\mathrm{e}^{2st}} \tag{12}$$

$$\mathrm{e}^{st}\doteq\frac{\mathrm{e}^{a}}{2\sinh(a-st)}=\frac{\mathrm{e}^{st}}{1-\mathrm{e}^{-2a}\mathrm{e}^{2st}} \tag{13}$$

The reciprocal hyperbolic functions can be expressed as an infinite sum of rational functions as follows [23]

$$\frac{1}{\cosh z}=2\pi\sum_{n=0}^{\infty}\frac{(-1)^n(n+1/2)}{(n+1/2)^2\pi^2+z^2} \tag{14}$$

$$\frac{1}{\sinh z}=\frac{1}{z}+2z\sum_{n=0}^{\infty}\frac{(-1)^n}{n^2\pi^2+z^2} \tag{15}$$

By using (12) to (15), the Bromwich contour integral can be calculated by residual theorem, thus, the approximate formula of the inverse Laplace transform can be expressed as [23]

$$f_c(t,a)=\frac{e^a}{t}\sum_{n=1}^{\infty}(-1)^n\,\mathrm{Im}\left[F\left(\frac{a}{t}+\mathrm{j}\left(n-\frac{1}{2}\right)\frac{\pi}{t}\right)\right] \tag{16}$$

$$f_s(t,a)=\frac{e^a}{t}\left\{\frac{1}{2}F\left(\frac{a}{t}\right)+\sum_{n=1}^{\infty}(-1)^n\,\mathrm{Re}\left[F\left(\frac{a}{t}+\mathrm{j}n\frac{\pi}{t}\right)\right]\right\} \quad (17)$$

where $f_c(t, a)$ and $f_s(t, a)$ are the approximate formula $f(t)$ by using the indirect algorithm of the numerical inverse Laplace transform of $F(s)$, of which the kernel is approximated by (12) and (13), respectively.

Under the condition of $a > ct$, (12) and (13) can be expanded as a convergent MacLaurin series, from which the absolute errors of (16) and (17) are as follows, respectively

$$\theta_c(t,a)=\sum_{n=1}^{\infty}(-1)^n\,\mathrm{e}^{-2na}f\left[(2n+1)t\right] \quad (18)$$

$$\theta_s(t,a)=\sum_{n=1}^{\infty}\mathrm{e}^{-2na}f\left[(2n+1)t\right] \quad (19)$$

where $\theta_c(t, a)$ and $\theta_s(t, a)$ are the absolute errors corresponding to $f_c(t, a)$ and $f_s(t, a)$, respectively.

The resultant error of the approximate formula can be further suppressed by taking the arithmetic mean of (16) and (17). Thus the approximate formula of the inverse Laplace transform can be expressed as

$$\begin{aligned}f_a(t,a)&=\frac{1}{2}\left[f_c(t,a)+f_s(t,a)\right]\\&=\frac{\mathrm{e}^a}{2t}\left(\frac{1}{2}F\left(\frac{a}{t}\right)+\sum_{n=1}^{\infty}(-1)^n\left\{\mathrm{Re}\left[F\left(\frac{a}{t}+\mathrm{j}n\frac{\pi}{t}\right)\right]+\right.\right. \quad (20)\\&\left.\left.\mathrm{Im}\left[F\left(\frac{a}{t}+\mathrm{j}\left(n-\frac{1}{2}\right)\frac{\pi}{t}\right)\right]\right\}\right)\end{aligned}$$

The corresponding absolute error is

$$\theta_a(t,a)=\sum_{n=1}^{\infty}\mathrm{e}^{-4na}f\left[(4n+1)t\right] \quad (21)$$

where $\theta_a(t, a)$ is the absolute error corresponding to $f_a(t, a)$.

This method is an indirect method to obtain the approximate formula of inverse Laplace transform by approximating the kernel of the inverse Laplace transform, rather than by directly discretizing the Bromwich contour integral expression. This method is firstly proposed by Valsa in 1998 [23]. Thus, this method is named as the indirect algorithm in the following part.

In general, the convergence of the series in the approximate formula is very poor, since the absolute value of its terms decreases for large n only in inverse proportion to n^2 and n of (17) and (16), respectively. To improve the convergence of the approximate formula, Euler transformation can be used [28, 29]. Euler transformation is especially effective with the series that originally had very bad convergence under the condition of (a) the signs of the series are alternating, (b) the absolute values of the terms decrease monotonically with increasing n.

In summary, the problem of calculation of response in the time domain is converted into the problem of calculation of complex frequency responses in the Laplace domain. Thus, many problems are thus simplified, for example, materials with frequency-dependent dielectric losses.

IV. Calculation Procedures for FEM in Complex Frequency Domain by Indirect Algorithm

The electric potential and the normal component of the electric field intensity on the Dirichlet boundary can be approximated by the approximate expression of the inverse Laplace transform. Then, each term of the in the series summation can be calculated by the finite element equation. For the electric potential, each term can be calculated by (6). While for the normal component of the electric field intensity on the Dirichlet boundary, each term can be calculated by (10). After obtaining the electric potentials at all instants, the electric field intensity at each instant can be obtained by taking the negative gradient of the electric potential at each instant. In summary, the flow diagram for calculating transient electric field by FEM in the complex frequency domain is illustrated in Fig. 2.

In the calculation, it is worth noting that the image function in the complex frequency domain of the boundary conditions needs to be analytic. If the image function of the boundary condition cannot be obtained analytically, the boundary condition can be expanded into trigonometric series, and then the image function of the trigonometric series can be obtained analytically.

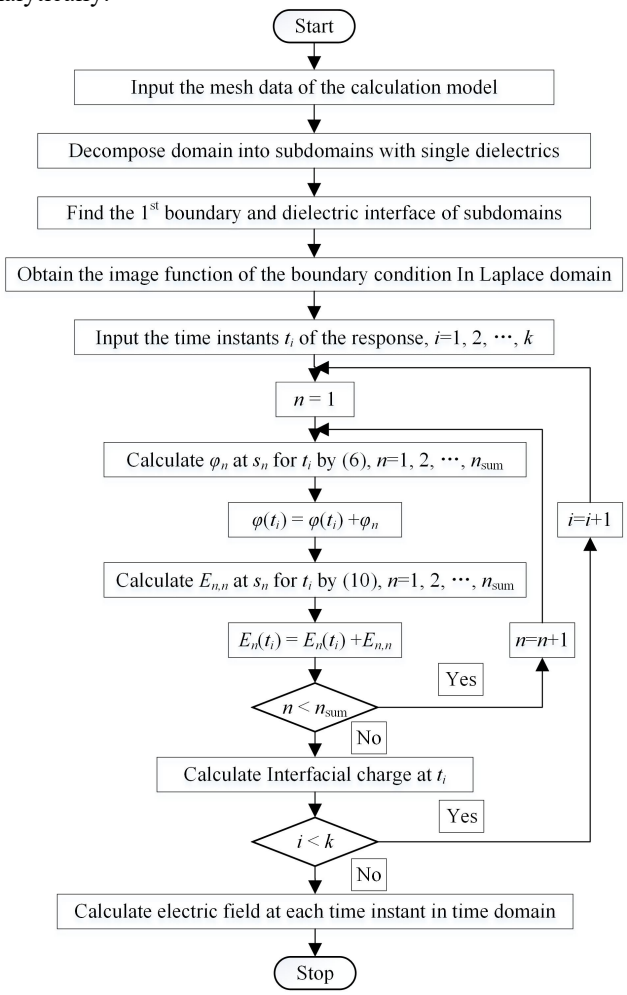

Fig. 2. Flow diagram for calculating transient electric field by FEM in the complex frequency domain

For the combined insulation structure with multiple materials,

the normal component of the electric field intensity on the dielectric interface is discontinuous, and interfacial charges will accumulate on the dielectric interface due to the discontinuity of the permittivity and conductivity of the materials. To calculate the normal component of the electric field intensity on the dielectric interface and interfacial charge density, special treatment needs to be arranged [27]. The filed domain Ω needs to be decomposed into several subdomains Ω_i with only one material. Thus, all dielectric interfaces between subdomain Ω_i and other subdomains and the Dirichlet boundary of subdomain Ω_i can be regarded as the equivalent Dirichlet boundary in subdomain Ω_i.

In subdomain Ω_i, the nodal potential at each complex frequency is obtained by (6) in the previous procedures. Then, the normal component of the transient electric field intensity at each complex frequency on the equivalent Dirichlet boundary of subdomain Ω_i can be calculated by (10). Repeating the above procedures for all subdomains, the normal component of the transient electric field intensities at each time step on the Dirichlet boundary and the dielectric interface of domain Ω can be solved.

V. Numerical Examples

A. Numerical Model

A classical model with double-layered dielectrics in series is selected for numerical calculation, as shown in Fig. 3. Dielectrics in the model are isotropic linear and homogeneous, which are labeled as 1 and 2. For the dielectric 1, the thickness, the permittivity, and the conductivity are d_1, ε_1, and γ_1, respectively. While for the dielectric 2, these parameters are d_2, ε_2, and γ_2, respectively. In the calculation, $d_1=d_2=1$ mm, $\varepsilon_{r1}=3.96$, $\gamma_1=2.55\times10^{-15}$ S/m, $\varepsilon_{r2}=2.26$, and $\gamma_2=1.04\times10^{-12}$ S/m, When $t = 0$, the switch is closed and the voltage $u_s(t)$ is applied across the two electrodes. The fringing effect is neglected, thus the fields in each dielectric are uniform [6].

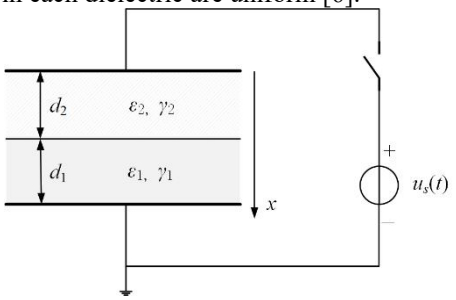

Fig. 3. Model of the composite structure with double-layer dielectrics[30]

B. The Step Response of the Transient Electric Field

The step response of the classical model in Fig. 3 is selected to evaluate the numerical error of the indirect algorithm since the step response of the classical model is analytical. Besides, the numerical result calculated by the direct algorithm is also compared.

The expression of the direct algorithm of the numerical inverse Laplace transform is expressed as [31]

$$f_n = \frac{\mathrm{e}^{cn\Delta t}}{t_{\max}} \mathrm{Re}\left[\sum_{k=0}^{N-1} F_k \mathrm{e}^{\mathrm{j}2\pi kn/N}\right] \tag{22}$$

where, c is the damping coefficient, Δt is the sampling interval of time, $t_{\max}$ is the maximum calculation time, N is the total number of the sampling points, n is the label of the discrete sequence of time, k is the label of the discrete sequence of complex frequency, F_k is the value of the image function $F(s)$ in the k^{st} complex frequency point s_k.

The damping coefficient c is recommended as [31]

$$\frac{1}{t_{\max}} \le c \le \frac{3}{t_{\max}} \tag{23}$$

The comparison of the step response of the transient electric field in dielectric 1 by the direct algorithm and indirect algorithm is depicted in Fig. 4. Among them, Fig. 4(a) is the comparison of the numerical results of electric field intensity, and Fig. 4(b) is the relative error of the electric field intensity.

In the calculation, the magnitude of the step voltage is $U_{\mathrm{m}}=1000$ V, and the maximum of the observing time is $t_{\max}=250$ s. For the direct algorithm of the FEM in complex frequency domain (CFD-FEM), $N=500$, $\Delta t=0.5$ s, $c=1/t_{\max}=0.004$. While for the indirect algorithm of the CFD-FEM, the numerical results are calculated by (20). Besides, the coefficient $a=3$, the number of terms in the series summation is $n_{\mathrm{s}}=20$, and the number of terms in the series summation by Euler transformation is $n_{\mathrm{d}}=20$.

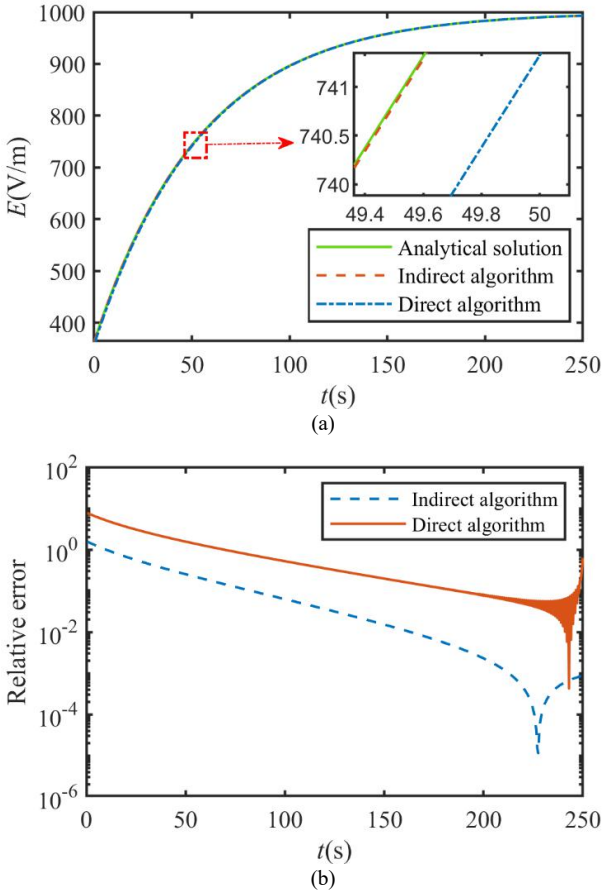

Fig. 4. Comparison of the step response of the transient electric field intensity in dielectric 1 by the direct algorithm and indirect algorithm, (a) magnitude of the electric field intensity, (b) relative error.

As shown in Fig.4(a), the numerical results by both direct algorithm and indirect algorithm have no numerical oscillations,

which can match well with the analytical solution. The relative error of the indirect algorithm is significantly lower than that of the direct algorithm by more than one order of magnitude when calculating the step response of the transient electric field, which is depicted in Fig.4(b).

C. The Zero-state Response of the Transient Electric Field under the PPSW Voltage

When t = 0, the switch is closed and the excitation voltage $u_s(t)$ is applied across the two electrodes. Initially, there is no unpaired charge between the electrodes either in the volume or on the interface. Under this condition, the response of the transient electric field is the zero-state response. In this section, the calculation of the zero-state response of the transient electric field is conducted under the positive periodic square waveform (PPSW) voltage.

The schematic figure of the PPSW voltage is depicted in Fig. 5, where, U_m is the magnitude of the PPSW voltage $u_s(t)$, t_u and t_d are the rise time and fall time of the PPSW voltage, respectively, α is the duty cycle, which is defined as the ratio of the duration of positive impulse voltage within a cycle to the duration of the cycle T_c is the cycle.

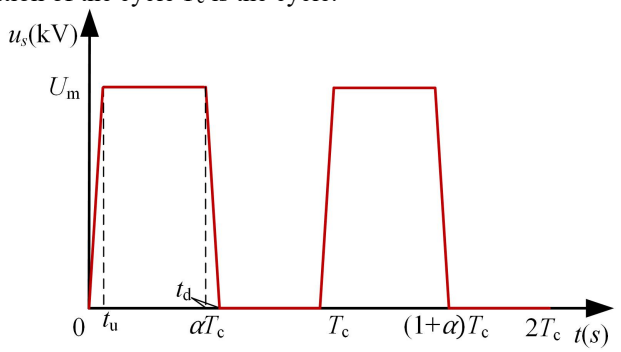

Fig. 5 Schematic of the positive periodic square waveform voltage [30]

The PPSW voltage $u_s(t)$ can be expressed as

$$u_s(t)=\sum_{i=0}^{\infty}u_T(t-iT_\mathrm{c}) \tag{24}$$

where, $u_T(t)$ is the expression of $u_s(t)$ when $t\in[0, \mathrm{T}]$, and $u_T(t)$ is expressed as

$$\begin{aligned}u_T(t)=&\left[tu(t)-(t-t_\mathrm{u})u(t-t_\mathrm{u})-(t-\alpha T_\mathrm{c})u(t-\alpha T_\mathrm{c})+\right.\\&\left.(t-\alpha T_\mathrm{c}-t_\mathrm{d})u(t-\alpha T_\mathrm{c}-t_\mathrm{d})\right]U_m\end{aligned} \tag{25}$$

By taking the Laplace transform of $u_T(t)$, the image function $U_T(s)$ can be obtained

$$U_T(s)=\frac{U_m}{s^2}\left(1-\mathrm{e}^{-t_r s}-\mathrm{e}^{-\alpha T s}+\mathrm{e}^{-(\alpha T+t_f)s}\right) \tag{26}$$

$$U_T(s)=\frac{U_m}{s^2}\left(1-\mathrm{e}^{-t_r s}-\mathrm{e}^{-\alpha T s}+\mathrm{e}^{-(\alpha T+t_f)s}\right) \tag{26}$$

By using the time-shift characteristics of the Laplace transform, the image function $U_s(s)$ of the PPSW voltage $u_s(t)$ in the complex frequency domain is

$$U_s(s)=U_m\frac{1}{s^2}\left(1-\mathrm{e}^{-t_r s}-\mathrm{e}^{-\alpha T s}+\mathrm{e}^{-(\alpha T+t_f)s}\right)\frac{1}{1-\mathrm{e}^{-Ts}} \tag{27}$$

The results of the zero-state response of the transient electric field in dielectric 1 under the PPSW voltage are shown in Fig. 6.

In the calculation, U_m=1000V, t_u=t_d=1 s, α=0.5, T_c=50 s. Different numerical results by the direct algorithm and indirect algorithm of the CFD-FEM and FEM in the time domain (TD-FEM) are compared. For higher numerical accuracy of the electric field intensity, in the calculation by TD-FEM, the transient constrained electric field equation on the boundary is adopted [27], and the time step is selected as Δt=0.5 s. Other calculation parameters of the direct algorithm and indirect algorithm of the CFD-FEM are the same as those in Section V-B.

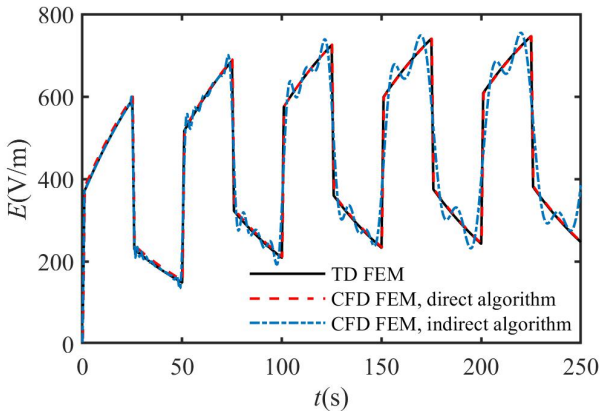

Fig. 6 Comparison of the zero-state response of the transient electric field under the PPSW voltage.

As shown in Fig. 6, the results by the direct algorithm of CFD-FEM can match well with the results by TD-FEM, and no numerical oscillation appears. While for the results by the indirect algorithm of CFD-FEM, the overall trend is consistent with the results by TD-FEM, but the numerical oscillation is obvious. In the first cycle, the numerical oscillation is very small, which can be ignored. However, the oscillation increases with time. The reason for the oscillation and the method to eliminate it will be explained in Section VI.

D. The Zero-input Response of the Transient Electric Field

The zero-input response refers to the response caused only by the initial state variables without external excitation. Based on Section V-C, supposing that the switch is opened at t=250 s, and the external excitation of the PPSW voltage is removed. Due to the effect of the applied voltage within 0 s<t<250 s, there are some interfacial charges on the dielectric interface, and the electric field is distributed in the medium at t=250 s. As a result, the calculation of the transient electric field after t>250 s is the problem of calculating the zero-input response of the transient electric field, where the initial state variable is the electric potential at t=250 s. The results of the zero-input response of the transient electric field in dielectric 1 are depicted in Fig. 7.

Different numerical results calculated by the direct algorithm and indirect algorithm of the CFD-FEM are compared in Fig. 7. The time duration for calculation is [250s, 500s]. Other calculation parameters of the direct algorithm and indirect algorithm of the CFD-FEM are the same as that of Section V-B.

As illustrated in Fig. 7, the overall trend of the transient electric field calculated by the direct algorithm and indirect algorithm of the CFD-FEM are almost the same, and the results can match well at the intermediate time duration. However, at

the beginning and the ending of the calculation time duration, the numerical results calculated by the direct algorithm have some numerical oscillations. While results calculated by the indirect algorithm do not show any numerical oscillations.

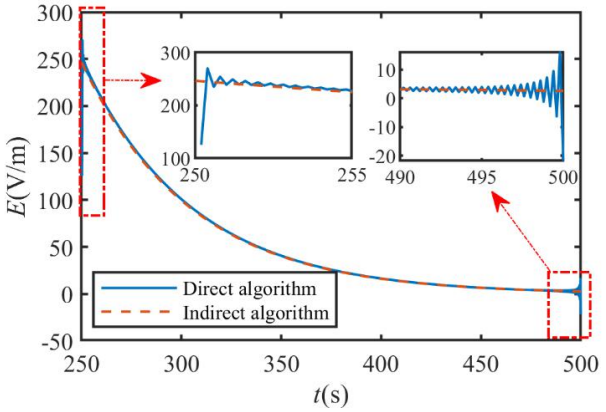

Fig. 7 Comparison of the zero-input response of the transient electric field.

VI. Discussions

As it can be seen from the numerical examples in Section V, the numerical accuracy of the indirect algorithm of the CFD-FEM is more than an order of magnitude higher than that of the direct algorithm. For solving the zero-input response of the transient electric field, the indirect algorithm will not produce any numerical oscillations. While for calculating the zero-state response under the periodic excitations, numerical oscillations will occur. This section aims to reduce this kind of numerical oscillation.

The approximate formula of the numerical inverse Laplace transform behaves like a low-pass filter, as illustrated in (16), (17), and (20). In actual calculations, the summation of the series is conducted for finite terms, which will filtrate high-frequency components of the response. As a result, numerical oscillations are produced inevitably. Intuitively speaking, increasing the number of terms in the summation of the series will reduce the numerical oscillations.

For the zero-state response of the transient electric field under the PPSW voltage in Section V-C, the response is calculated under a different number of terms in the summation of the series, which is shown in Fig. 8.

As illustrated in Fig. 8, oscillations appear in the 1st cycle when n_s=20, and n_d=20. When the number of terms increases by n_s=100 and n_d=20, oscillations occur in the 3rd cycle. And when the number of terms further increase by n_s=150 and n_d=20, oscillations only emerge in the 5th cycle. Moreover, the oscillations are very small, which can be almost neglected. Thus, these results in Fig. 8 confirm the conjecture that the oscillations can be reduced by increasing the number of terms for the summation of the series in the approximate formulas.

In the actual calculations, the number of the terms for summation cannot be obtained through a continuous test by trial, because it may cause much calculation time. Thus, how to quantitatively select the number of items for summation will be discussed in the following.

In the approximate formulas, for each time instant of t, the angular frequency of the last complex frequency point for the calculation is

$$\omega = \frac{n\pi}{t} = 2\pi f \tag{28}$$

where, f is the corresponding frequency.

Suppose the cut-off frequency of the transient response of the electric field which needs to be solved $f(t)$ within a specific truncation error limit is f_c. To obtain $f(t)$ within a specific error limit from $F(s)$ by the approximate formula, the frequency of the last complex frequency point for calculation should not be less than f_c. As a result, n should satisfy

$$n \geq 2tf_c \tag{29}$$

If we want to obtain $f(t)$ in the time interval $[0, t_{\max}]$, the total number of items in the series summation n_{sum} should satisfy

$$n_{\text{sum}} \geq 2t_{\max} f_c \tag{30}$$

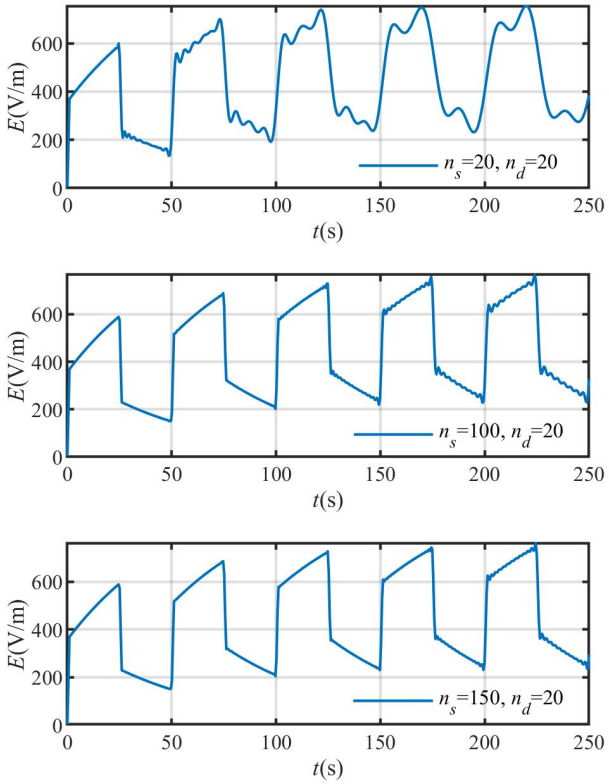

Fig. 8. Zero-state response of the transient electric field under the PPSW voltage with a different number of terms in the summation of the series.

To evaluate the cut-off frequency of the response of the electric potential within a specific truncation error limit, the image function of the response can be written as

$$\varphi_{\text{L}}(s) = U_s(s)H(s) = \frac{U_s(s)}{\gamma + \varepsilon s} \tag{31}$$

where, $\varphi_{\text{L}}(s)$ is the image function of response $\varphi(t)$ in the complex frequency domain, $U_s(s)$ is the image function of the excitation voltage $U_s(t)$, $H(s)$ is the transfer function, and for the transient electric field in the EQS field, $H(s)=1/(\gamma+\varepsilon s)$.

Thus, the cut-off frequency of the $\varphi(t)$ can be obtained from the frequency spectrum corresponding to the $\varphi_{\text{L}}(s)$. The cut-off frequency is selected as the frequency point in which the amplitude of the spectrum attenuates to 1% of the maximum

magnitude of the spectrum. For the composite insulation structure with multiple materials, if there are multiple media in the field, corresponding to each media, the cutoff frequency of $\varphi(t)$ is calculated respectively corresponding to the parameters of each media. Then, the maximum cut-off frequency is chosen as the cut-off frequency of $\varphi_L(s)$.

The frequency spectrum corresponding to $\varphi_L(s)$ with different parameters is depicted in Fig. 9, where the blue line and the red line are frequency spectrum with parameters in dielectric 1 and 2, respectively. As shown in Fig. 9, the cut-off frequency is selected as f_c=1 Hz.

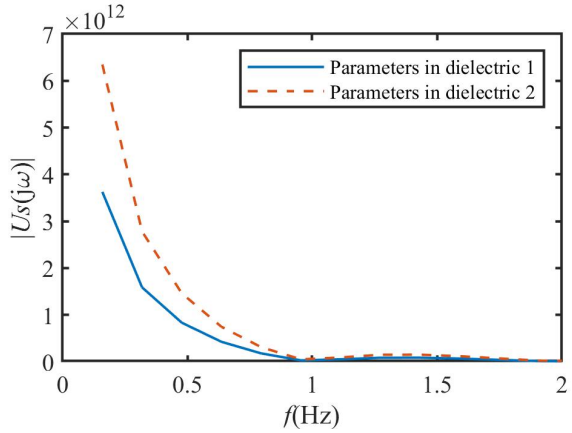

Fig. 9. Frequency spectrum corresponding to $\varphi_L(s)$.

Thus, the total number of items in the series summation n_{sum} can be obtained by (26), i.e. $n_{sum}\geq 500$. The calculation results are shown in Fig. 10, where, a=3, n_s=500, and n_d=20.

As shown in Fig. 10, the numerical oscillations are almost eliminated, compared with that in Fig. 8. And even in the last cycle, there is no obvious oscillation in the result. Thus, it proves the effectiveness of the proposed method for reducing oscillations. It can be testified that the proposed method for selecting the total number of items in the series summation n_{sum} is effective.

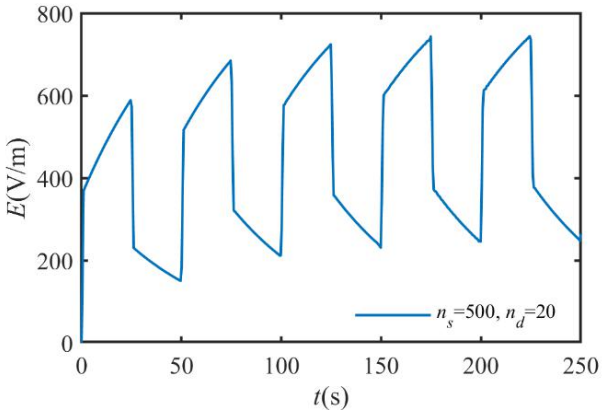

Fig. 10. Zero-state response of the transient electric field under the PPSW voltage with n_{sum}=500.

The premise of reducing oscillations is to increase the computational cost. To reduce the total computation cost, the following suggestion can be adopted. Before calculating time response at $t=t_k$, increase an additional procedure to calculate the minimum of $n_{sum}(t_k)$ by

$$n_{\text{sum}}(t_k) = 2t_k f_c \tag{32}$$

That is to say, the number of terms of the summation of the series is varying with time. And the total computational cost will be reduced by half.

To testify the effectiveness of the proposed method of the time-varying number of terms of the summation, the calculation results of the zero-state response of the transient electric field under the PPSW voltage are depicted in Fig. 11, which is compared with the calculation results with the definite number of terms of the summation in Fig. 10.

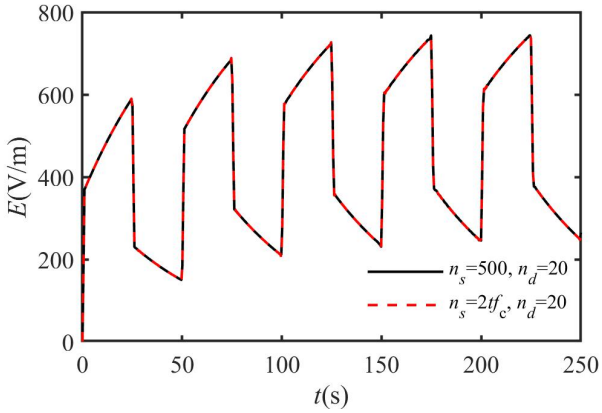

Fig. 11. Zero-state response of the transient electric field under the PPSW voltage with time-varying number of terms of the summation.

As shown in Fig. 11, the calculation results with the time-varying number of terms of the summation are matched well with the calculation results with the definite number of terms of the summation. To quantitatively describe the difference between the zero-state response of the transient electric field under the PPSW voltage with the time-varying number of terms of the summation and the definite number of terms of the summation, respectively, the relative error is depicted in Fig, 12. The relative error is calculated based on the numerical results with the definite number of terms of the summation.

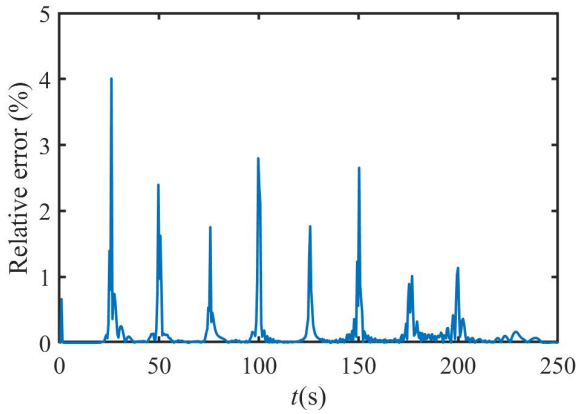

Fig. 12. Relative error of the zero-state response of the transient electric field under the PPSW voltage with time-varying number of summation terms.

The maximum of the relative error is 4.01%, as shown in Fig. 12, which is acceptable in engineering. Besides, the average relative error in the whole calculation time is just 0.15%. Moreover, the calculation cost of the numerical results calculated with the time-varying number of terms of the

summation is decreased by 52.51% compared with that of the numerical results calculated with the definite number of terms of the summation. It can be proved that using the proposed time-varying number of terms of the summation for calculations can reduce the calculation cost by a little more than a half while ensuring a relatively small error, which is acceptable and practical in engineering calculation.

VII. Application

To apply the proposed method to the actual engineering model, the transient electric field of the actual model is conducted by the proposed indirect algorithm of the CFD-FEM.

The actual insulation structure of direct bonded copper (DBC) structure is the main insulation structure used in the press-packed insulated gate bipolar transistor (IGBT). The voltage applied to the DBC structure under the actual working condition is the PPSW voltage. In the calculation, the magnitude of the PPSW voltage is U_m=18kV, the frequency of the voltage is f=50Hz, the duty cycle is α=0.5, the rise time and fall time of the voltage is t_r=t_f=2μs, the total calculation time is 200s. These waveform parameters are corresponding to a typical working voltage of the Silicon carbide (SiC) based press-packed IGBT device for the power grid application.

For the typical working voltage of the SiC based press-packed IGBT, the cut-off frequency is selected as f_c=10 Hz. Thus, n_s in the calcalation is selected as n_s=20t_k accoring to (32). Besides, n_d=20, and a=3, which are selected as the same with those in Section VI.

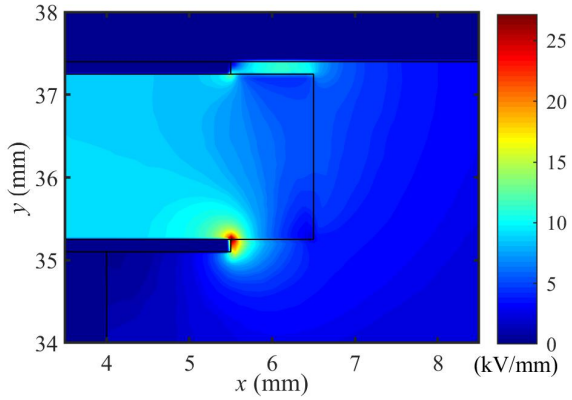

(a)

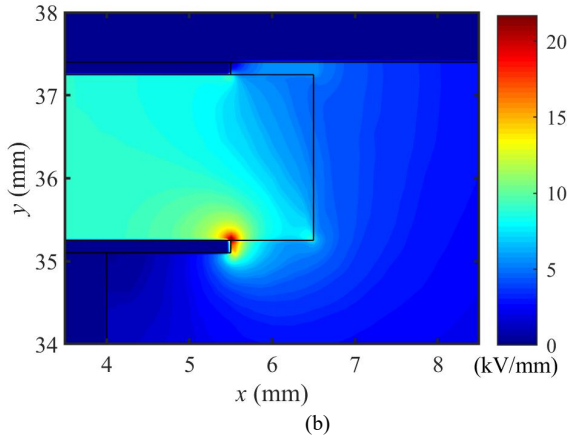

(b)

Fig. 13. Distribution of the transient electric field at the end of the off-state in different cycle, (a) the first cycle, (b) the last cycle.

To display the calculation results, the distributions of the transient electric field at the end of the off-state in different cycle are shown in Fig. 13. The contour of the electric field in the first cycle and in the last cycle are depicted in Fig. 13(a) and Fig. 13(b), respectively.

The transient electric field and the interfacial charge density at selected point is illustrated in Fig. 14, in which the Fig. 14(a) and Fig. 14(b) are the electric field intensity and interfacial charge density varying with time, respectively.

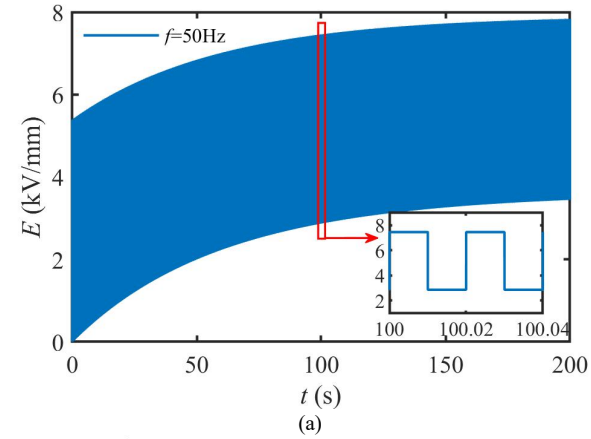

(a)

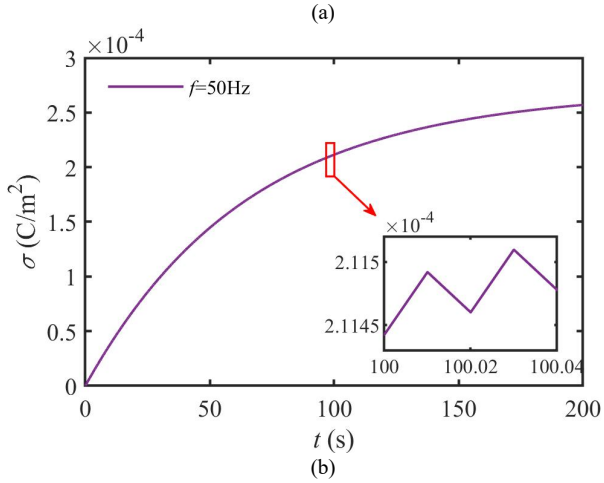

(b)

Fig. 14. The transient electric field and the interfacial charge density at selected point, (a) electric field intensity, (b) interfacial charge density..

As shown in Fig. (13) and Fig. (14), these calculation results reflect the transient characteristics of the electric field and interfacial charge density of the DBC structure under the PPSW voltage. It also can be testified the validity of the proposed indirect algorithm of the CFD-FEM to the actual model.

VIII. Conclusions

This paper proposes an indirect algorithm for the finite element method in the complex frequency domain (CFD-FEM), the main conclusions are as follows.

(1) CFD-FEM is proposed for the transient electric field under electroquasistatic field by using the indirect algorithm of the inverse numerical Laplace transform. CFD-FEM can calculate the transition process under periodic excitation and the zero-input response caused by the initial conditions, which

solves the problem that the FEM in the frequency domain can only calculate the periodic steady-state response, but cannot calculate the transition process.

(2) The indirect algorithm of the CFD-FEM has higher numerical accuracy than that of the direct algorithm. Besides, the indirect algorithm solves the problem of numerical oscillation of the zero-input response by the direct algorithm CFD-FEM. However, when calculating the zero-state response under periodic excitation, the indirect algorithm will produce numerical oscillation, and the numerical oscillation gradually increases with time.

(3) In order to reduce numerical oscillations by the indirect algorithm when calculating the zero-state response under periodic excitation, the method of choosing the number of terms for summations of the series in the approximate formula is proposed in this paper. In addition, choosing the number of terms for summations of the series which is time-varying for each time, selecting the number of summations can reduce the computational cost by nearly a half while reducing the numerical oscillation.

APPENDIX

The expression of stiffness matrix $\mathbf{S}_k$ is written as

$$\mathbf{S}_k = \mathbf{K}_\gamma + s\mathbf{K}_\varepsilon \tag{A1}$$

where $\mathbf{K}_\gamma$ and $\mathbf{K}_\varepsilon$ are the stiff matrixes corresponding to the conductivity and the permittivity respectively. Expressions for $\mathbf{K}_\gamma$, and $\mathbf{K}_\varepsilon$, can be given as

$$\mathbf{K}_\gamma = \sum_{j=1}^{n}\sum_{\mathrm{e}=1}^{m}\int_{\Omega_\mathrm{e}} \gamma \nabla N_i^\mathrm{e} \bullet \nabla N_j^\mathrm{e}\,\mathrm{d}\Omega \tag{A2}$$

$$\mathbf{K}_\varepsilon = \sum_{j=1}^{n}\sum_{\mathrm{e}=1}^{m}\int_{\Omega_\mathrm{e}} \varepsilon \nabla N_i^\mathrm{e} \bullet \nabla N_j^\mathrm{e}\,\mathrm{d}\Omega \tag{A3}$$

Stiffness matrix $\mathbf{T}$ and column vector $\mathbf{F}_k$ are expressed as

$$\mathbf{T} = \mathbf{K}_\varepsilon \tag{A4}$$

$$\begin{aligned}\mathbf{F}_k = &\sum_{\mathrm{e}=1}^{m_2}\int_{\Gamma_{2\mathrm{e}}} \left[\gamma + (c + \mathrm{j}2\pi k\Delta f)\varepsilon\right] N_i^\mathrm{e}\psi_{lk}\,\mathrm{d}\Gamma - \\ &\sum_{\mathrm{e}=1}^{m_1}\int_{\Gamma_{1\mathrm{e}}} \left[\gamma + (c + \mathrm{j}2\pi k\Delta f)\varepsilon\right] N_i^\mathrm{e}E_{nlk}\,\mathrm{d}\Gamma + \\ &\sum_{\mathrm{e}=1}^{m_1}\int_{\Gamma_{1\mathrm{e}}} \varepsilon N_i^\mathrm{e}E_{nt}(0_-)\,\mathrm{d}\Gamma - \sum_{\mathrm{e}=1}^{m_2}\int_{\Gamma_{2\mathrm{e}}} \varepsilon N_i^\mathrm{e}\psi_t(0_-)\,\mathrm{d}\Gamma\end{aligned} \tag{A5}$$

Each element in $\mathbf{F}_k$ can be expressed as

$$f_{ki} = \begin{cases} 0 & i \text{ in } \Omega \\ \sum_{\mathrm{e}=1}^{m_2}\int_{\Gamma_{2\mathrm{e}}} \left[\gamma + (c + \mathrm{j}2\pi k\Delta f)\varepsilon\right] N_i^\mathrm{e}\psi_{lk}\,\mathrm{d}\Gamma - & \\ \qquad \sum_{\mathrm{e}=1}^{m_2}\int_{\Gamma_{2\mathrm{e}}} \varepsilon N_i^\mathrm{e}\psi_t(0_-)\,\mathrm{d}\Gamma & i \in \Gamma_2 \\ -\sum_{\mathrm{e}=1}^{m_1}\int_{\Gamma_{1\mathrm{e}}} \left[\gamma + (c + \mathrm{j}2\pi k\Delta f)\varepsilon\right] N_i^\mathrm{e}E_{nlk}\,d\Gamma + & \\ \qquad \sum_{\mathrm{e}=1}^{m_1}\int_{\Gamma_{1\mathrm{e}}} \varepsilon N_i^\mathrm{e}E_{nt}(0_-)\,\mathrm{d}\Gamma & i \in \Gamma_1 \end{cases} \tag{A6}$$

Each element of the stiffness matrixes $\mathbf{H}_k$ and $\mathbf{G}$ are expressed as

$$h_{ki,j} = \sum_{e=1}^{m_1}\int_{\Gamma_{1e}} (\gamma + s\varepsilon) N_i^\mathrm{e} N_j^\mathrm{e}\,\mathrm{d}\Gamma \tag{A7}$$

$$g_{ij} = \sum_{e=1}^{m_1}\int_{\Gamma_{1e}} \varepsilon N_i^\mathrm{e} N_j^\mathrm{e}\,\mathrm{d}\Gamma \tag{A8}$$

where, $i, j = n_1+1, \cdots, n$, n_1 is the number of nodes on the Dirichlet boundary, and m_1 is the number of elements on the Dirichlet boundary.

REFERENCES

[1] E. Deng *et al.,* "Analysis on the difference of the characteristic between high power IGBT modules and press pack IGBTs," *Microelectron. Reliab.*, vol. 78, pp. 25–37, 2017.

[2] S. Arumugam, S. Gorchakov, and T. Schoenemann, "Dielectric and partial discharge investigations on high power insulated gate bipolar transistor modules," *IEEE Trans. Dielectr. Electr. Insul.*, vol. 22, no. 4, pp. 1997–2007, 2015.

[3] R. Simpson *et al.,* "Press-pack IGBTs for HVDC and FACTS," *CSEE J. Power Energy Syst.*, vol. 3, no. 3, pp. 302–310, 2017.

[4] P. Fu *et al.*, "The role of time-lag in the surface discharge inception under positive repetitive pulse voltage," *Phys. Plasmas*, vol. 25, no. 9, pp. 1–9.

[5] P. Fu *et al.*, "Partial discharge measurement and analysis in PPIs," *IET Power Electron.*, vol. 12, no. 1, pp. 138–146, Jan. 2019.

[6] H. A. Haus and J. R. Melcher, *Electromagnetic fields and energy*. Englewood Cliffs, NJ: Prentice-Hall, 1989.

[7] T. Chandrupatla and A. Belegundu, *Introduction to finite elements in engineering.* Cambridge University Press, 2021.

[8] O. C. Zienkiewicz, R. L. Taylor, and J. Z. Zhu, *The finite element method: its basis and fundamentals*, 6th ed. Oxford: Elsevier, 2005.

[9] S. Hiruma and H. Igarashi, "Time-domain analysis of homogenized finite-element method for eddy current analysis with reduced unknown variables," *IEEE Trans. Magn.*, vol. 56, no. 1, pp. 1-4, 2020.

[10] Y. Takahashi *et al.*, "Parallel time-periodic finite-element method for steady-state analysis of rotating machines," *IEEE Trans. Magn.*, vol. 48, no. 2, pp. 1019–1022, 2012.

[11] L. Qi, X. Cui, Z. Zhao, and H. Li, "Grounding performance analysis of the substation grounding grids by finite element method in frequency domain," *IEEE Trans. Magn.*, vol. 43, no. 4, pp. 1181–1184, 2007.

[12] F. Sheng, H. Gan, and D. Jiao, "Fast iterative solution algorithms in the frequency-domain layered finite element method for analyzing integrated circuits," *IEEE Trans. Adv. Packag.*, vol. 33, no. 2, pp. 524–533, 2010.

[13] H. S. Tsay and F. H. Yeh, "Finite element frequency-domain acoustic analysis of open-cell plastic foams," *Finite Elem. Anal. Des.*, vol. 42, no. 4, pp. 314–339, 2006.

[14] P. Jose, R. Kanapady, and K. K. Tamma, "Transform domain based hybrid element formulations for transient electromagnetic field computations," *C. Model. Eng. Sci.*, vol. 5, no. 5, pp. 409–421, 2004.

[15] R. J. Beerends, H. G. ter Morsche, J. C. Van den Berg, and E. M. Van de Vrie, *Fourier and Laplace transforms*. New York: Cambridge University Press, 2003.

[16] A. M. Cohen, *Numerical methods for Laplace transform inversion*, vol. 5. New Yor: Springer Science & Business Media, 2007.
[17] P. Moreno and A. Ramirez, "Implementation of the numerical Laplace transform: A review," *IEEE Trans. Power Deliv.*, vol. 23, no. 4, pp. 2599–2609, 2008.
[18] P. Gomez and F. A. Uribe, "The numerical Laplace transform: An accurate technique for analyzing electromagnetic transients on power system devices," *Int. J. Electr. Power Energy Syst.*, vol. 31, no. 2–3, pp. 116–123, 2009.
[19] B. Davies, *Integral transforms and their applications*, 3rd ed. New York: Springer Science & Business Media, 2005.
[20] H. Stehfest, "Algorithm 368: Numerical inversion of Laplace transforms [D5]," *Commun. ACM*, vol. 13, no. 1, pp. 47–49, 1970.
[21] W. T. Weeks, "Numerical inversion of Laplace transforms using Laguerre functions," *J. ACM*, vol. 13, no. 3, pp. 419–429, 1966.
[22] A. Talbot, "The accurate numerical inversion of Laplace transforms," *IMA J. Appl. Math.*, vol. 23, no. 1, pp. 97–120, 1979.
[23] J. Valsa and L. Brančik, "Approximate formulae formula for numerical inversion of Laplace transforms," *Int. J. Numer. Model. Electron. Networks, Devices Fields*, vol. 11, no. 3, pp. 153–166, 1998.
[24] L. Brančík and N. Smith, "Two approaches to derive approximate formulae formula of NILT method with generalization," in 2015 38*th International Convention on Information and Communication Technology, Electronics and Microelectronics (MIPRO)*, 2015, pp. 155–160.
[25] E. Morales-Casique and S. P. Neuman, "Laplace-transform finite element solution of nonlocal and localized stochastic moment equations of transport," *Commun. Comput. Phys.*, vol. 6, no. 1, p. 131, 2009.
[26] E. A. Sudicky and R. G. McLaren, "The Laplace transform Galerkin technique for large-scale simulation of mass transport in discretely fractured porous formations," *Water Resour. Res.*, vol. 28, no. 2, pp. 499–514, 1992.
[27] T. Wen, *et al.*, "A time-domain finite element method for the transient electric field and transient charge density on the dielectric interface," *CSEE J. Power Energy Syst.*, pp. 1–11, 2020, On line.
[28] R. G. Stanton, *Numerical methods for science and engineering*. Prentice-Hall, 1961.
[29] T. Hosono, "Numerical inversion of Laplace transform and some applications to wave optics," *Radio Sci.*, vol. 16, no. 6, pp. 1015–1019, 1981.
[30] T. Wen *et al.* "Characterization of electric field distribution within high voltage press-packed IGBT submodules under condition of repetitive turn-on and turn-off," *CSEE J. Power Energy Syst.*, 2021, Accepted.
[31] T.wen *et al.*, "Finite element method in complex frequency domain for transient electric field intensity under electro-quasistatic field," *Proc. CSEE*, under review (in Chinese).

Teng Wen was born in Hunan Province, China, in 1991. He received his B.Sc. degree in Electrical Engineering from North China Electric Power University, Beijing, China, in 2013. He is a Ph.D. candidate in Electrical Engineering at North China Electric Power University now. His main research interests include computational electromagnetics, electrical insulation, and packaging problems for high voltage power semiconductor devices.

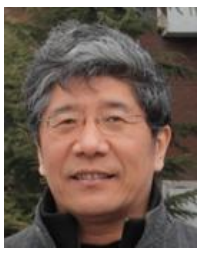

Xiang Cui (M'97–SM'98) was born in Baoding, Hebei Province, China, in 1960. He received his B.Sc. and M.Sc. degrees in Electrical Engineering from North China Electric Power University, Baoding, in 1982 and 1984, respectively, and his Ph.D. degree in Accelerator Physics from the China Institute of Atomic Energy, Beijing, China, in 1988. He is currently a Professor and the Vice Director of the State Key Laboratory of Alternate Electrical Power System with Renewable Energy Sources, North China Electric Power University. His research interests include computational electromagnetics, electromagnetic environment, and electromagnetic compatibility in power systems, insulation, and magnetic problems in high-voltage apparatus. Prof. Cui is a Standing Council Member of the China Electrotechnical Society, a Fellow of *IET*, a Senior Member of *IEEE*. He is also an Associate Editor of *IEEE Transactions on Electromagnetic Compatibility*.

Xuebao Li was born in Tianjin, China, in 1988. He received his B.Sc. degree and Ph.D. degree in Electrical Engineering from North China Electric Power University, Beijing, China, in 2011 and 2016, respectively. He is currently an associate professor at the School of Electrical and Electronic Engineering, North China Electric Power University. His research interests include the electromagnetic environment and electromagnetic compatibility in power systems and insulation problems in high-voltage apparatus.

Sijia Liu was born in Hubei Province, China, in 1997. She received her B.Sc. degree in Electrical engineering from North China Electric Power University, Beijing, China, in 2020, where she is currently pursuing her M.Sc. degree in Electrical Engineering. Her main research interest is computational electromagnetics, electrical insulation, and packaging problems for high voltage power semiconductor devices.

Zhibin Zhao was born in Hebei, China, in 1977. He received his Ph.D. degree in Electrical Engineering from North China Electric Power University, Baoding, China, in 2005. Currently, he is a Professor at the State Key Laboratory of Alternate Electrical Power System with Renewable Energy Sources, North China Electric Power University. His main research interests include computational electromagnetics and electromagnetic compatibility in power electronics.